Atmospheric Research 116 (2012) 22–32

Contents lists available at ScienceDirect

Atmospheric Research

journal homepage: www.elsevier.com/locate/atmos

Fast retrieval of aerosol optical depth and its sensitivity to surface albedo using remote sensing data

F.C. Seidel [a,*], A.A. Kokhanovsky [b], M.E. Schaepman [a]

[a] Remote Sensing Laboratories, University of Zurich, Winterthurerstr. 190, 8057 Zurich, Switzerland
[b] Institute of Environmental Physics, University of Bremen, O. Hahn Allee 1, 28334 Bremen, Germany

ARTICLE INFO

Article history:
Received 7 December 2010
Received in revised form 16 March 2011
Accepted 18 March 2011

Keywords:
Aerosol retrieval
Remote sensing
Radiative transfer
Surface albedo
Atmosphere
Sensitivity

ABSTRACT

Aerosol remote sensing over land is still a great challenge. The retrieval of optical and micro-physical aerosol properties usually requires comprehensive and computationally extensive retrieval algorithms. An efficient approach for the retrieval of the aerosol optical depth (AOD) is proposed in this paper. It is based on a fast and simple atmospheric radiative transfer model using approximations and analytical equations. The proposed algorithm is validated on both synthetic data from the benchmark radiative transfer model SCIATRAN and on real data from the airborne imaging spectrometer APEX. The promising results confirm the feasibility of retrievals using single wavelength nadir observations under constrained conditions. The AOD retrieval is found to be very sensitive to uncertainties in the surface albedo. In the current experimental setup, 0.01 surface albedo uncertainty leads to approximately 0.2 AOD retrieval uncertainty. Generally, larger AOD leads to the increase of reflectance R at sensor level for underlying "dark" surfaces and to a decrease of R for "bright" surfaces. R does not depend strongly on AOD for a surface albedo in the range of approximately 0.2–0.4. Third and higher orders of aerosol scattering, polarization and three-dimensional effects at the surface–atmosphere interface are not taken into account by this study. Nevertheless, a brief validation shows the feasibility with promising results of the proposed simple and fast AOD retrieval algorithm from remote sensing data.

1. Introduction

Aerosols are important to our climate (Charlson et al., 1992; Rind et al., 2009) and health (Wilson and Spengler, 1996). According to the intergovernmental panel on climate change (IPCC), some changes in the energy budget are still difficult to understand due to key uncertainties in local radiative forcing by aerosols and related feedback mechanisms (Solomon et al., 2007). Remote sensing and radiative transfer (RT) models are important instruments for determining micro-physical and optical aerosol properties and better understanding the impact of aerosols on climate (Rind et al., 2009). The aerosol optical depth (AOD) is one of the most often retrieved optical properties. It describes the proportion of the extinction (scattering and absorption) of solar light due to aerosols (Ångström, 1930; van de Hulst, 1948). Operational AOD retrieval algorithms are well established using data from MODIS with the "dark target" approach (*e.g.* Levy et al., 2007) or the Deep Blue algorithm (*e.g.* Hsu et al., 2004), from MISR (*e.g.* Diner et al., 2005; Martonchik et al., 2009), OMI (Torres et al., 2007) and other sensors (*e.g.* Tanré, 2010). Still, uncertainties exist mainly due to sub-pixel clouds and approximations regarding effects of the surface (Levy et al., 2010). There are few studies available using airborne high spatial resolution imagers for aerosol retrievals on the local scales (Bassani et al., 2010). Nonetheless, precise measurements of aerosol scattering are of vital importance to the atmospheric correction of such data (Guanter et al., 2005; Gao et al., 2009).

The retrieval of AOD from remote sensing data is performed by RT model inversion. The number of concurrent

* Corresponding author.
E-mail address: felix.seidel@geo.uzh.ch (F.C. Seidel).

0169-8095/$ – see front matter © 2011 Elsevier B.V. All rights reserved.
doi:10.1016/j.atmosres.2011.03.006

independent measurements is usually lower than the number of unknowns, which requires ancillary information or assumptions to constrain such a problem. For example, *a priori* knowledge of the spectral bidirectional reflectance function (BRDF) of the underlying surface and its surrounding area is needed to account for three-dimensional effects at the surface (Lyapustin, 2001). Concurrent measurements of all these variables are currently not available and assumptions on the surface properties and the aerosol model have to be made to constrain the problem. A recent intercomparison study by Kokhanovsky et al. (2010b) has shown that existing retrieval algorithms may retrieve slightly different values of AOD, even when applied to simulated data on black surfaces. Remote sensing of aerosol over land will remain a challenging retrieval problem.

In this paper, we propose a fast and simple AOD retrieval algorithm. The inverse Simple Model for Atmospheric Radiative Transfer (iSMART) is based on approximate analytical solutions of the RT problem. Its minimal complexity and fast computation are important assets for the processing of large datasets, such as imaging spectrometer data. Fast and approximate estimates of AOD permit the prior calculation of probability density functions (PDF), which are used to reduce the ill-conditioned nature of the inverse approach in biophysical parameter modeling, for example. Naturally, computational speed comes at the expense of accuracy, but might still be within the expected uncertainty envelope of comparable algorithms (*e.g.* MODIS AOD retrieval over land Remer et al., 2005; Levy et al., 2009). Another fast, albeit more extensive approach to AOD retrieval was published by Katsev et al. (2010), which is again based on a fast RT model (see Kokhanovsky and de Leeuw (2009), p. 101–134).

This paper describes an AOD retrieval algorithm. It is validated in Sections 4.1 and 4.2 using synthetic and real airborne remote sensing data respectively, which are introduced in Section 3. iSMART is used in Section 4.3 to investigate the effect of the critical surface albedo and uncertainties of surface albedo on AOD retrievals.

2. iSMART — inverse Simple Model for Atmospheric Radiative Transfer

Spectral radiances L_λ are measured by optical remote sensing instruments and can be simulated by RT models. We approximate L_λ as a function of the optical depth of molecules and aerosols $\tau_\lambda = \tau_\lambda^{mlc} + \tau_\lambda^{aer}$, the scattering phase function $P_\lambda(\Theta)$ at scattering angle Θ, single-scattering albedo ω_λ, surface albedo a_λ, cosine of solar and viewing zenith angles (SZA and VZA) μ_0 and μ, and finally the relative azimuth between viewing and solar direction $\phi - \phi_0$. The subscript λ denotes wavelength dependence. τ_λ^{aer} can be derived from one L_λ value under the condition that all other parameters are known or estimated.

The reflectance values:

$$R_\lambda = \frac{\pi L_\lambda}{\mu_0 F_{0,\lambda}} \tag{1}$$

will be used below, where $F_{0,\lambda}$ is the spectral solar irradiance.

2.1. Radiative transfer model

A Simple Model for Atmospheric Radiative Transfer (SMART) is proposed and validated by Seidel et al. (2010). It is based upon analytical equations, parameterizations and a correction factor for molecular multiple scattering to provide fast computations. The accuracy is in the order of 5–10% for typical observational conditions and up to 15% for combinations of large SZA and high AOD in the blue spectral range.

Assuming a sensor at top-of-atmosphere (TOA) and a surface albedo a_λ, R_λ is given by:

$$\begin{aligned} R_\lambda^{TOA} = & \underbrace{\underbrace{\frac{P^{mlc}(\Theta)}{4(\mu_0+\mu)}\left(1-e^{-\tau_\lambda^{mlc}\left(\frac{1}{\mu_0}+\frac{1}{\mu}\right)}\right)}_{R_\lambda^{SSA;mlc}} f_{\mu_0}^{corr}}_{R_\lambda^{mlc}} \\ & + \underbrace{\underbrace{\frac{\omega_\lambda^{aer} P_\lambda^{aer}(\Theta)}{4(\mu_0+\mu)}\left(1-e^{-\tau_\lambda^{aer}\left(\frac{1}{\mu_0}+\frac{1}{\mu}\right)}\right)}_{R_\lambda^{SSA;aer}} + R_\lambda^{2^{nd}S;aer}}_{R_\lambda^{aer}} \\ & + \underbrace{T_\lambda^{\downarrow}\frac{a_\lambda}{1-s_\lambda a_\lambda}T_\lambda^{\uparrow}}_{R_\lambda^{SFC}}. \end{aligned} \tag{2}$$

The molecular reflectance R_λ^{mlc} is the product of the single-scattering approximation (*SSA*) $R_\lambda^{SSA;mlc}$ and a generic correction factor $f_{\mu_0}^{corr}$ per SZA to approximate molecular multiple scattering. The latter is derived from prior MODTRAN/DISORT (Stamnes et al., 1988; Berk et al., 1989) calculations (Seidel et al., 2010). The Rayleigh scattering phase function for unpolarized solar radiation is given by:

$$P^{mlc}(\Theta) = \frac{3}{4}\left(1 + cos^2\Theta\right) \tag{3}$$

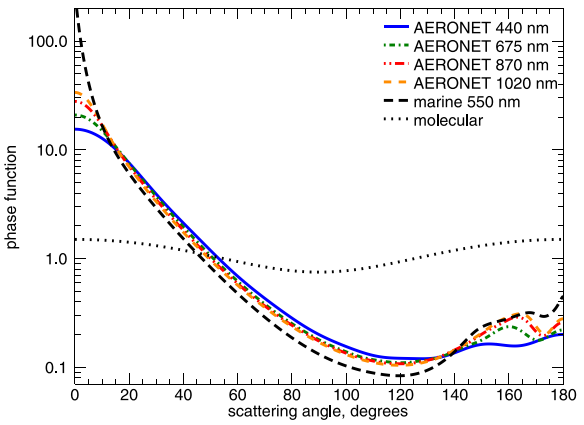

Fig. 1. Phase functions $P_\lambda(\Theta)$ as function of the scattering angle Θ for molecular (Eq. 3) and aerosol scattering. The latter is calculated for marine particles using Lorenz–Mie scattering theory (see Section 3.1) and derived from AERONET measurements (see Section 3.2).

(see Fig. 1), where

$$\Theta = arccos\left[\pm\mu_0\mu + cos(\phi-\phi_0)\sqrt{(1-\mu_0^2)(1-\mu^2)}\right] \quad (4)$$

is the forward (+) or backward (−) scattering angle. The aerosol reflectance approximation R_λ^{aer} is the sum of the first order scattering $R_\lambda^{SSA;aer}$ and the second order scattering $R_\lambda^{2^{nd}S;aer}$ according to the successive orders of scattering method as formulated by Hansen and Travis (1974):

$$\begin{aligned} R_\lambda^{2^{nd}S;aer}(\mu,\mu_0,\phi-\phi_0) = {} & \frac{\omega_\lambda^{aer}\tau_\lambda^{aer}}{4\pi} \\ & \cdot\int_0^{2\pi}\int_0^{1}\left[\frac{1}{\mu}P_\lambda^{T;aer}(\mu,\mu',\phi-\phi')R_\lambda^{SSA;aer}(\mu',\mu_0,\phi'-\phi_0)\right. \\ & + \frac{1}{\mu_0}R_\lambda^{SSA;aer}(\mu,\mu',\phi-\phi')P_\lambda^{T;aer}(\mu',\mu_0,\phi'-\phi_0) \\ & - \frac{e^{-\frac{\tau_\lambda^{aer}}{\mu_0}}}{\mu_0}T_\lambda^{SSA;aer}(\mu,\mu',\phi-\phi')P_\lambda^{aer}(\mu',\mu_0,\phi'-\phi_0) \\ & \left. - \frac{e^{-\frac{\tau_\lambda^{aer}}{\mu}}}{\mu}P_\lambda^{aer}(\mu,\mu',\phi-\phi')T_\lambda^{SSA;aer}(\mu',\mu_0,\phi'-\phi_0)\right]d\mu'd\phi'. \end{aligned} \quad (5)$$

$P_\lambda^{aer}(\Theta)$ is calculated according to the Lorenz–Mie scattering theory. $P_\lambda^{T;aer}$ denotes the transmittance phase function using the forward scattering angle of Eq. (4). van de Hulst (1948), Sobolev (1972), Hansen and Travis (1974), Kokhanovsky (2006) and others derived an analytical equation for the aerosol single-scattering transmittance:

$$T_\lambda^{SSA;aer} = \frac{\omega_\lambda^{aer}P_\lambda^{aer}(\Theta)}{4(\mu_0-\mu)}\left(e^{-\frac{\tau_\lambda^{aer}}{\mu_0}}-e^{-\frac{\tau_\lambda^{aer}}{\mu}}\right), \quad (6)$$

or in case of $\mu_0=\mu$:

$$T_\lambda^{SSA;aer} = \frac{\omega_\lambda^{aer}P_\lambda^{aer}(\Theta)}{4\mu^2}\tau_\lambda^{aer}e^{-\frac{\tau_\lambda^{aer}}{\mu}}. \quad (7)$$

Eq. (5) allows approximating the total aerosol scattering exclusively by using SSA equations (see Eqs. (2) and (6)) integrated over the scattering directions μ and ϕ. R_λ^{SFC} in Eq. (2) describes the reflectance function of an underlying homogeneous Lambertian surface according to Ångström (1925), Chandrasekhar (1960), Sobolev (1972) and others with the surface albedo a_λ, the spherical albedo s_λ of the atmosphere for illumination from below as well as the total down and upward transmittance $T_\lambda^{\downarrow}$ and $T_\lambda^{\uparrow}$, respectively. A parameterization with respect to τ_λ^{aer} and the asymmetry parameter g for s_λ, $T_\lambda^{\downarrow}$ and $T_\lambda^{\uparrow}$ was used as suggested in Kokhanovsky et al. (2005).

Seidel et al. (2010) provides a complete description of SMART including an extended formulation of Eq. (2) for airborne remote sensing and a validation with 6S (Vermote et al., 1997).

Fig. 2 shows calculations of R_{550nm}^{TOA} using SMART (lines) at $a_{550nm}\in[0.0(0.2)1.0]$. Corresponding benchmark results using SCIATRAN (Rozanov et al., 2005) are plotted as reference (circles). Both models were run independently using the same phase function for marine aerosols as described in Section 3.1 and shown in Fig. 1. A good agreement between both models was found for $a_{550nm}\leq 0.8$ and $\tau_{500nm}^{aer}\leq 0.5$. SMART is generally less accurate in the blue spectral region due to neglected coupling of molecular and higher orders of aerosol scattering, as well as polarization effects.

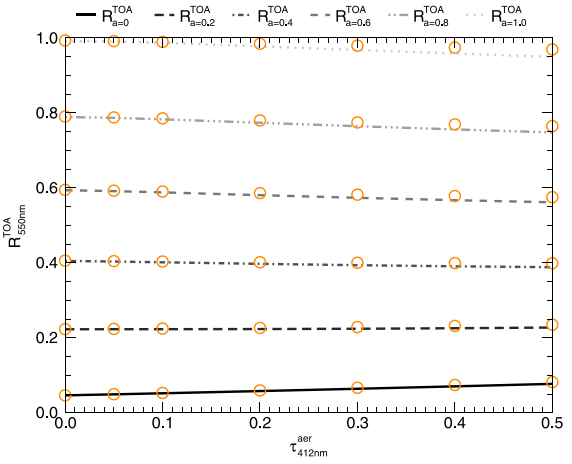

Fig. 2. Reflectance R_{550nm}^{TOA} as a function of AOD for surface albedo $a_{550nm}\in[0.0(0.2)1.0]$. The lines were computed by Eq. (2) and the circles by using SCIATRAN as a benchmark. AOD inputs are given in Table 1. Both models used the same marine aerosol phase function (see Section 3.1 and Fig. 1).

2.2. AOD retrieval with iSMART

iSMART is an extended version of SMART, which was developed for AOD retrievals from radiance measurements. iSMART initiates repeated SMART runs, until convergence with measured data is achieved. It uses *a priori* knowledge of a_λ, aerosol particle size distribution (PSD) and spectral aerosol refractive indices. The method uses the following Boolean function:

$$\begin{aligned} & \left(R_{\tau_\lambda^{aer}}^{SMART} < R_{\tau_\lambda^{aer}=?}^{Data} \leq R_{\tau_\lambda^{aer}+i}^{SMART}\right) \\ & \qquad \vee \\ & \left(R_{\tau_\lambda^{aer}}^{SMART} > R_{\tau_\lambda^{aer}=?}^{Data} \geq R_{\tau_\lambda^{aer}+i}^{SMART}\right) \end{aligned} \quad (8)$$

to search for the optimal solution with respect to the best fit between data and model. iSMART uses a decision tree with heuristically selected branches (see Fig. 3) allowing fast convergence on the most likely solution, which defines the AOD to be retrieved ($\tau_\lambda^{aer}=?$). The AOD interval between two branches is defined by: $i=j\cdot 2^{(1-h)}$, where $h\in[1,2,3,4]$ is the hierarchy and j is the initial AOD interval in the top hierarchy ($h=1$). Thus, each subsequent hierarchy narrows down the search using halved AOD intervals. We used $j=0.2$ and started the procedure at $\tau_\lambda^{aer}=0.0$ and $\tau_\lambda^{aer}+i=0.2$. If the conditions of Eq. (8) are met, the search in the subsequent hierarchy continues between $\tau_\lambda^{aer}=0.0$ and $\tau_\lambda^{aer}+i=0.1$ or $\tau_\lambda^{aer}=0.1$ and $\tau_\lambda^{aer}+i=0.2$ (see Fig. 3). Else, the search is continued in the same hierarchy between $\tau_\lambda^{aer}=0.2$ and $\tau_\lambda^{aer}+i=0.4$, and so forth. Note that $R_{\tau_\lambda^{aer}}<R_{\tau_\lambda^{aer}+i}$ is usually found over dark surfaces and $R_{\tau_\lambda^{aer}}>R_{\tau_\lambda^{aer}+i}$ over bright surfaces (see

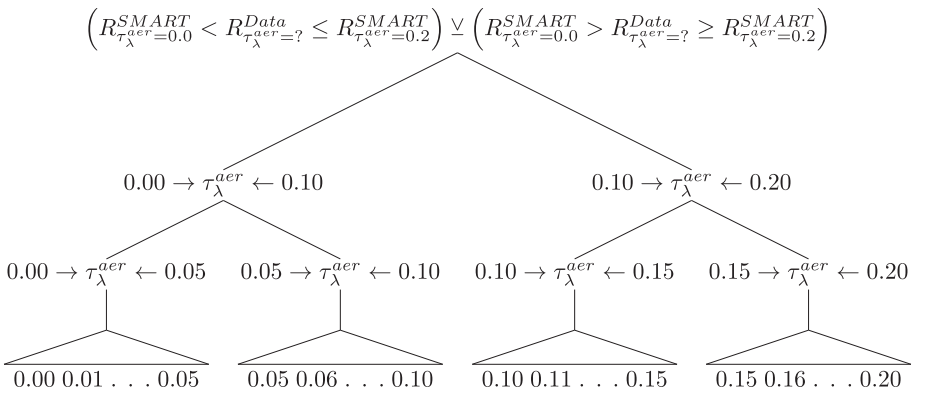

Fig. 3. Part of the decision tree used in iSMART to retrieve AOD with a sampling interval of 0.01. It shows the case where Eq. (8) fulfills the condition with an initial AOD interval between 0.0 and 0.2. Boolean functions are used to quickly find the optimal solution without interpolation.

Sections 4.1 and 4.3.1). After the initiation of the search, each step requires only one additional iteration, because one of the bounds is already known. In the lowest hierarchy ($h=4$), only four out of six calculations are needed, because both bounds are already known. This leads to a minimum of eight consecutive SMART iterations. If $\tau^{aer}_\lambda > 0.2$ then the next node in the first hierarchy tests with one additional calculation at $\tau^{aer}_{550nm}=0.4$ if the data fits the AOD interval $\tau^{aer}_\lambda \in [0.2, 0.4]$. If this is true, nine iterations are needed in total to find AOD, else one additional iteration per interval is needed. Twelve SMART iterations are needed to find an AOD, which is $\tau^{aer}_\lambda \in [0.8, 1.0]$. The AOD sampling interval is 0.01 and there is no interpolation of the results involved. $j=0.2$ was chosen because $\tau^{aer}_\lambda \in [0.0, 0.2]$ represent typical vales for Western Europe (Ruckstuhl et al., 2008).

The current version of iSMART requires that the function from R^{Data}_λ to R^{SMART}_λ is bijective. Therefore, both sets of R_λ have to be a monotonically increasing or decreasing function with respect to AOD. If ambiguous solutions exist, such that one R^{Data}_λ can be related to more than one R^{SMART}_λ, the retrieval algorithm (Eq. 8) may choose a wrong branch in the decision tree (Fig. 3). Results with $\tau^{aer}_\lambda \notin [0.00, 1.20]$ are rejected.

SMART calculates approximately 20 results per second on a current CPU (Seidel et al., 2010). The retrieval of one AOD value, including non-RT operations, requires approximately between 0.5 ($\tau^{aer}_\lambda \in [0.0, 0.2]$) and 0.8 s ($\tau^{aer}_\lambda \in [1.0, 1.2]$).

Other retrievals are possible as well (*e.g.* surface albedo), though not implemented in the current version of iSMART. Multi-directional measurements are required to simultaneously retrieve AOD and surface albedo.

3. Data

3.1. Synthetic data

We used a synthetic dataset for testing the retrieval algorithm under controlled conditions. It was computed using the independent benchmark RT model SCIATRAN (Rozanov and Kokhanovsky, 2006; Kokhanovsky et al., 2010a; b). The inherent accuracy of SCIATRAN is better than 1% relative error as compared with other RT models (Kokhanovsky et al., 2010a).

The synthetic dataset accounts for a standard atmosphere comprising non-absorbing marine aerosols and an underlying Lambertian surface with monochromatic surface albedos $a_\lambda \in [0.0(0.1)1.0]$. Gaseous absorption is ignored. The SZA is 60° and the VZA is 0° (nadir). The aerosol PSD is modeled using the log-normal law:

$$f(r) = \frac{1}{\sqrt{2\pi}\sigma r} exp\left[-\frac{ln^2(r/r_0)}{2\sigma^2}\right], \quad (9)$$

where r is the radius of the spherical homogeneous particles. The geometrical radius $r_0 = r_m exp(\sigma^2) = 100$ nm is assumed with a modal radius $r_m = 37$ nm and $\sigma = 1$. The effective radius and effective variance are defined in case of Eq. (9) as follows: $r_{ef} = r_0 exp(2.5\sigma^2) = 1218$ nm and $v_{ef} = exp(\sigma^2) - 1 = 1.7$ (Kokhanovsky, 2008, p. 5). The spectral extinction K^{ext}_λ and phase function $P^{aer}_\lambda(\Theta)$ are calculated using Lorenz–Mie scattering theory (Kokhanovsky, 2008). $P^{aer}_{550nm}(\Theta)$ is shown by the dashed line in Fig. 1. ω^{aer}_λ and the aerosol asymmetry parameter g^{aer} are set to 1.0 and 0.775, respectively. Reference values for the AOD retrieval using the synthetic dataset are given in Table 1. See Kokhanovsky (2008, p. 2–6) and Kokhanovsky et al. (2010b) for details on complete input parameters. The R^{Data}_{550nm} values of the synthetic dataset are shown in Fig. 2 (circles).

3.2. Airborne remote sensing data

Measurements provide realistic data to validate the proposed AOD retrieval algorithm. We use data acquired by the imaging spectrometer Airborne Prism Experiment (APEX) (Itten et al., 1997; 2008; Schaepman et al., 1998) and concurrent *in-situ*

Table 1
τ^{aer}_λ denotes the spectral aerosol optical depth as input to the computation of the synthetic data using SCIATRAN as well as benchmark to evaluate the retrieval accuracy of iSMART. See Kokhanovsky (2008, p. 2–6) and Kokhanovsky et al. (2010b) for further input parameters.

λ,nm	τ^{aer}_λ					
412	0.0500	0.1000	0.2000	0.3000	0.4000	0.5000
550	0.0498	0.0995	0.1990	0.2986	0.3981	0.4976
865	0.0467	0.0935	0.1870	0.2805	0.3739	0.4674

Table 2
APEX instrument specifications (Itten et al., 1997; 2008; Schaepman et al., 1998).

Type of instrument	Dispersive push-broom imaging spectrometer
Spectral range	380–2500 nm
Spectral bands (binned)	313
Spectral sampling interval	0.5–10 nm
Spectral resolution (FWHM)	0.6–11 nm
Spatial pixels	1000
Field of view (FOV)	28°
Spatial resolution	1.75 m at 3500 m a.g.l.

reflectance measurements of surface reference targets in addition to independent aerosol reference data.

The latter were measured *in-situ* by the nearby Aerosol Robotic Network (AERONET, Holben et al., 1998) sunphotometer (Laegern; 47°28.6N, 8°21.9E; 735 m a.m.s.l.). The radiative properties of the aerosols during the APEX overflight are given in Table 3. The PSD was derived from AERONET inversions (Dubovik and King, 2000) using Eq. (9) with $r=193$ nm, $r_0=214$ nm and $\sigma=0.45$. $P_\lambda^{aer}(\Theta)$ was determined using Lorenz–Mie scattering theory with the PSD as shown in Fig. 1. It should be noted that there was a hazy atmosphere with a presumably high aerosol concentration during the data acquisition.

The in-situ measurements of the surface reflectance were collected during the APEX overflight using portable field spectrometers (see Fig. 4). Each reference target is larger than nine APEX pixels (roughly 28 m^2; see Fig. 5b to e).

Table 2 provides the main APEX instrument specifications. Data were acquired in June 2010 close to Zurich, Switzerland (47°28.0N, 8°18.6E; 390 m a.m.s.l.). A true color subset of the data is shown in Fig. 5 with zooms on the surface reference targets.

4. Results

4.1. AOD retrieval accuracy using synthetic data

The use of synthetic data (see Section 3.1 and Table 1) is important for an initial evaluation of iSMART's accuracy. In this formal study, we use the same input values $P_\lambda^{aer}(\Theta)$, ω_λ^{aer} and surface albedo a as they were used for the SCIATRAN benchmark calculations. We assess the absolute error of the retrieved AOD using iSMART as follows:

$$\Delta\tau_\lambda^{aer} = \tau_\lambda^{aer,SCIATRAN} - \tau_\lambda^{aer,iSMART}. \quad (10)$$

Table 3
Independent in-situ measurements of optical and micro-physical aerosol properties from the Laegern AERONET site. τ_λ^{mlc} and τ_λ^{aer} denote the spectral molecular and aerosol optical thickness, respectively. ω_λ^{aer} is the aerosol single-scattering albedo and g^{aer} the aerosol asymmetry parameter.

λ, nm	τ_λ^{mlc}	τ_λ^{aer}	Refractive index	ω_λ^{aer}	g_λ^{aer}
440	0.224	0.619	$1.437-1.57^{-3}i$	0.990	0.732
675	0.039	0.304	$1.424-1.56^{-3}i$	0.987	0.664
870	0.014	0.185	$1.426-1.55^{-3}i$	0.985	0.601
1020	0.007	0.119	$1.422-1.55^{-3}i$	0.982	0.558

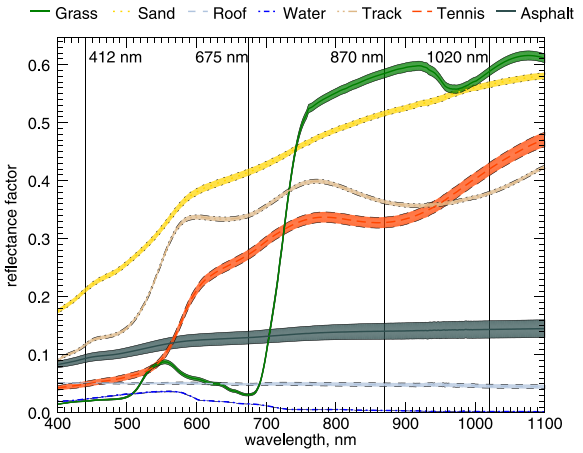

Fig. 4. Measured reflectance factor of the surface reference targets. The variability is represented by ±1 standard deviation around the average reflectance factor. The vertical lines denote the wavelengths for AOD retrieval.

The results are shown in Fig. 6 as a function of AOD and in Fig. 7 as a function of surface albedo. The expected uncertainty of the MODIS "dark-target" AOD retrieval algorithm over land is given as a reference in the same figures. It is defined by: $\pm0.05\pm0.15\tau_\lambda^{aer}$ valid at $a\leq0.25$ (Remer et al., 2005; Levy et al., 2009; 2010). The aerosol optical properties are *a priori* known from the input parameters used to prepare the synthetic data.

Fig. 6a provides $\Delta\tau_\lambda^{aer}$ (Eq. 10) for a dark surface with $a=0.1$. The error is small and mostly within the MODIS uncertainty envelope at all investigated wavelengths and AOD values. The small AOD overestimation is caused mainly due to the underestimation of R^{TOA} by the aerosol scattering approximation (Eq. 5). The analysis shows larger $\Delta\tau_\lambda^{aer}$ for $a=0.2$ (Fig. 6b) and 0.3 (Fig. 6c). The AOD is still overestimated by iSMART in the case of $a=0.2$, except for 865 nm and $\tau_{412nm}^{aer}\leq0.1$, where negative AOD values were rejected. iSMART strongly overestimates AOD at 412 nm and underestimates at 865 nm in case of $a=0.3$. At 550 nm, there is a change from under- to overestimation for $\tau_\lambda^{aer}\in[0.3,0.4]$. The errors are large, because R_λ^{TOA} is a very weak function of AOD at these surface albedos and the AOD retrieval is therefore very sensitive to small uncertainties, especially of surface albedo. This effect is discussed in Section 4.3.1. An example for results over brighter surfaces with $a\geq0.4$ are shown in Fig. 6d with an underestimation of retrieved AOD. $\Delta\tau_\lambda^{aer}$ is within the MODIS expected uncertainties for typical AOD values, except for the results at 412 nm.

Fig. 7 shows the same results as a function of a to emphasize the effect of surface albedo on the retrieval. The retrievals at 550 nm and 865 nm are mostly within the MODIS expected uncertainties. It is obvious that the combination of short wavelengths ($\lambda\leq500$ nm) with $a\geq0.2$ leads to larger $\Delta\tau_\lambda^{aer}$ because the error due to SMART's scattering approximations is amplified by a. The influence of $a\approx0.3$ on AOD retrievals (see Figs. 6c and 7) is further analyzed in Section 4.3.1.

It may be noted that most land surfaces are generally dark in the blue part of the solar spectrum (see Fig. 4). The results

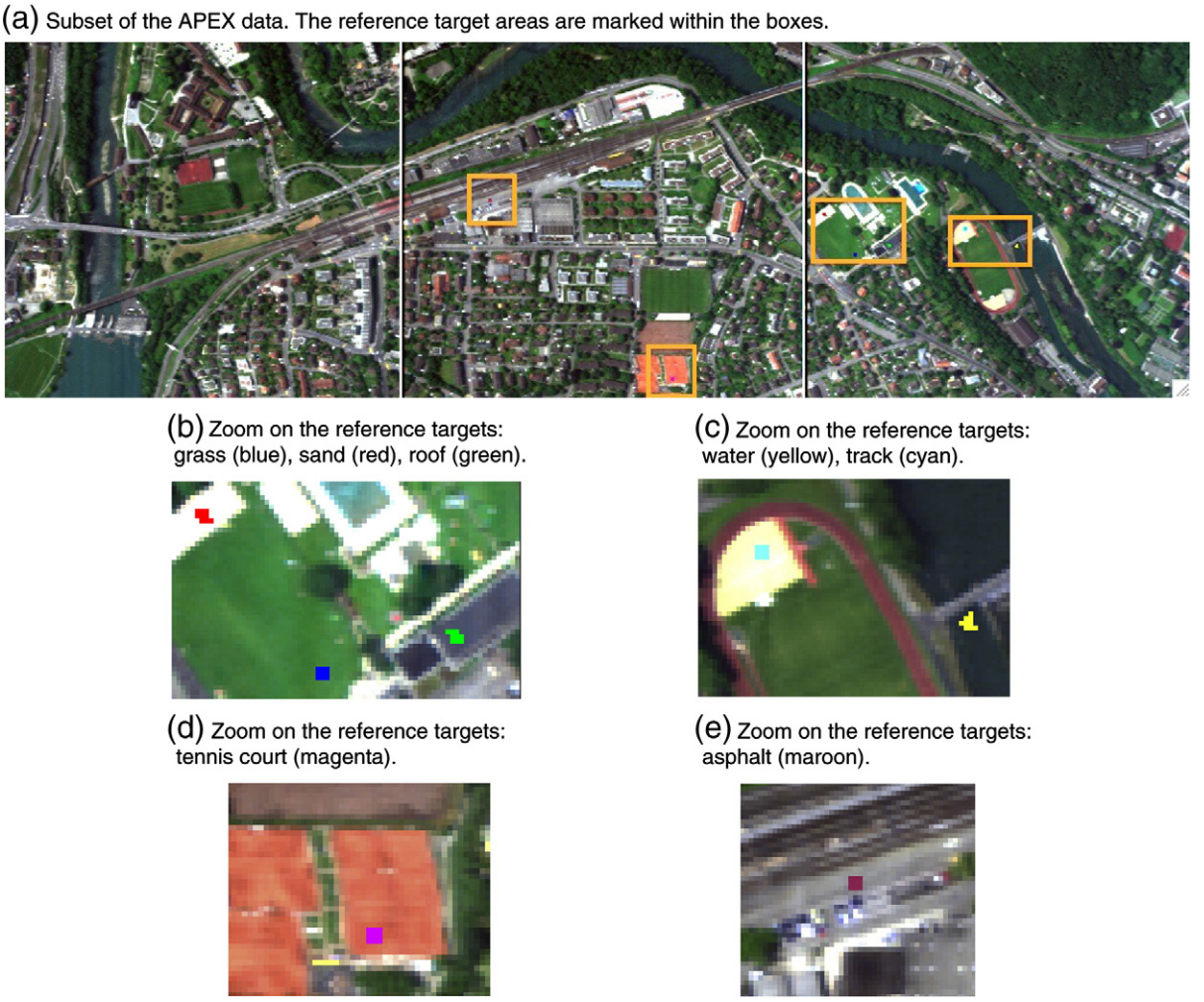

Fig. 5. Subset of the APEX data with the surface reference targets in true color.

of $\Delta\tau^{aer}_{412\mathrm{nm}}$ at $a>0.2$ in Figs. 6 and 7 are therefore more of theoretical interest.

4.2. AOD retrieval accuracy using airborne remote sensing data

The combined effects of all influences on the AOD retrieval were analyzed using airborne imaging spectrometer data, as well as surface and aerosol reference measurements (see Section 3.2). APEX's high spectral and spatial resolution data show that even water and artificial surfaces contain spectral features of *e.g.* vegetation due to adjacency effects by the hazy and strongly scattering atmosphere. We approximate this effects using the following simple linear forward mixing model for surface albedo with empirical coefficients: $a = a_{target} \cdot 0.8 + a_{surround} \cdot 0.2$, where $a_{surround}$ is estimated from the image data within a radius of 200 m around the targets.

Fig. 8 shows AOD results inverted from APEX data using iSMART. The aerosol reference data were measured by AERONET on a nearby hill, which is 380 m above the APEX data. The measured AOD values (solid line) are therefore extrapolated to the level of the image data using the RT model 6S (dotted line). These results show that iSMART is feasible to determine AOD from APEX data. However, there is a relatively large spread in the retrieved AOD at 440 nm due to SMART's scattering approximations as well as neglected aerosol–molecule coupling and polarization. The results at 675 nm deviate significantly when using the in-situ reference targets sand, track and tennis court. Interestingly, these targets have an $a_{675\mathrm{nm}}$ in the range of 0.25–0.4, which has already been found to be difficult for the AOD retrieval (see Fig. 7 and Sections 4.1 and 4.3.1). Longer wavelengths provide good results, which is a further agreement to the previous findings in Section 4.1.

4.3. Sensitivity of the AOD retrieval to surface albedo

In the following, we analyze the sensitivity of the AOD retrieval to surface albedo using again the synthetic data introduced in Section 3.1.

4.3.1. Critical surface albedo

AOD retrieval problems are found in Figs. 6 and 7 for $a \approx 0.3 \pm 0.1$. For about the same a, there is almost no

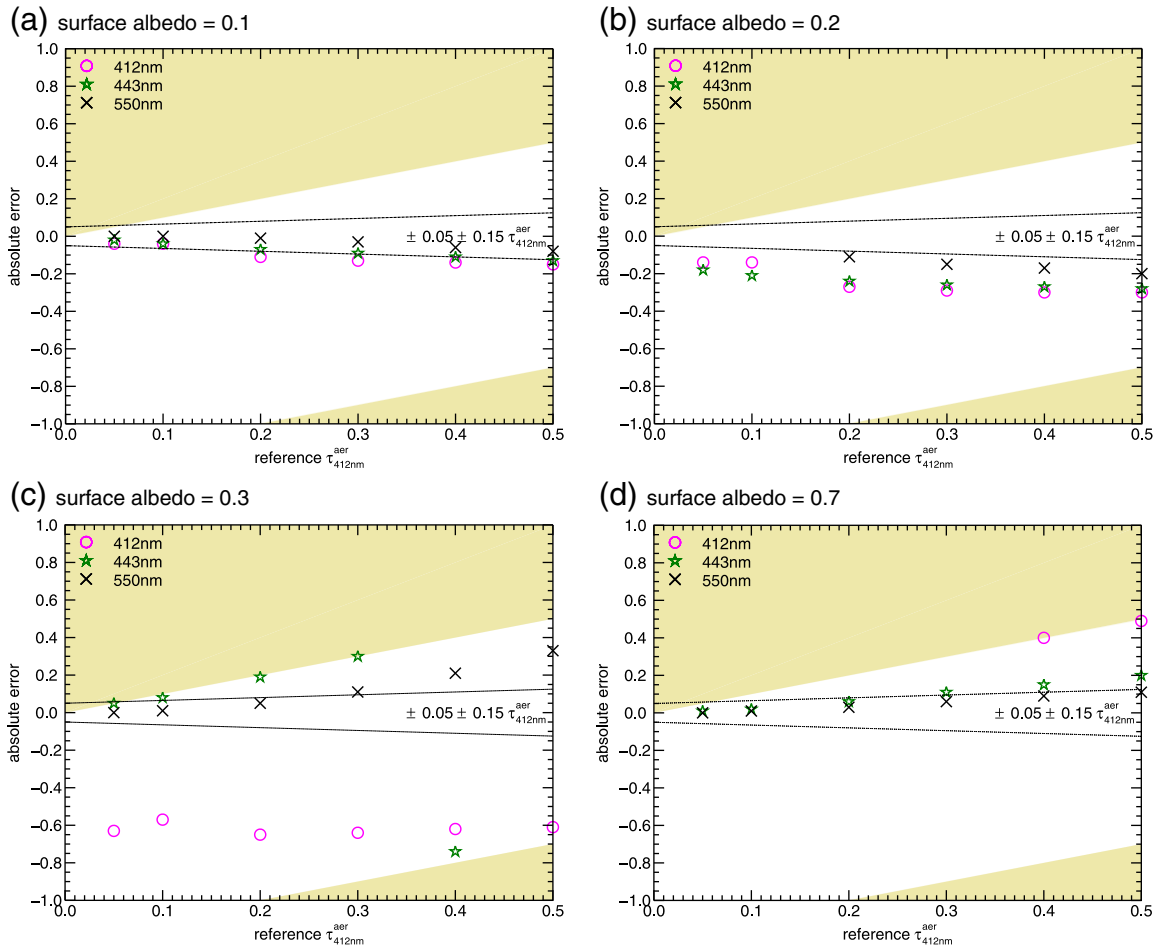

Fig. 6. Absolute error of AOD retrieval as a function of AOD. Calculations were performed using iSMART and compared to SCIATRAN. Retrievals in colored areas are not feasible because either $\tau^{aer}_{412nm}<0$ or $\tau^{aer}_{412nm}>1.2$. The dotted lines denote the expected uncertainty range of the MODIS dark-target ($0.01 \le a \le 0.25$) AOD retrieval.

influence of AOD on R^{TOA}_{550nm} (see Fig. 2). Such a is therefore posing difficulties for the AOD retrieval. The term critical surface albedo (CSA) was used in that sense by Fraser and Kaufman (1985), Hsu et al. (2004), Popp et al. (2007), Seidel et al. (2008), Zhu et al. (2011) and others. An example for the CSA is shown in Fig. 9 around $a_{550nm}=0.3$, where all SMART calculations for $\tau^{aer}_{550nm} \in [0.0(0.2)0.6]$ provide almost the same R^{TOA}_{λ}. The aerosol absorption and backward scattering are reducing the transmittance at the same time as the forward scattering is increasing the signal from the atmosphere. Fig. 9 shows also that additional AOD increases R^{TOA}_{λ} for $a<CSA$ and *vice versa* (see also Fig. 2). Thus, the net effect is positive at dark surfaces, negative at bright surfaces and zero at $a=CSA$. The CSA depends mainly on ω^{aer}_{λ} (Fraser and Kaufman, 1985; Popp et al., 2007), K^{ext}_{λ}, μ_0, μ, λ and slightly on aerosol particle concentration (Zhu et al., 2011).

To understand better the relationship between R^{TOA}_{λ}, τ^{aer}_{λ} and a_{λ}, we use the derivative of the reflectance with respect to AOD:

$$\frac{dR^{TOA}_{\lambda}}{d\tau^{aer}_{\lambda}} \begin{cases} > 0 & \text{if aerosols increase reflectance.} \\ = 0 & \text{if aerosols have no effects on reflectance.} \\ < 0 & \text{if aerosols decrease reflectance.} \end{cases} \quad (11)$$

for different surface albedos. The results using Eq. (11) are given in Fig. 10, where aerosols increase R^{TOA} at all $a \le 0.2$ and *vice versa* at $a \ge 0.3$. The aerosol effect on R^{TOA} is small for $a = 0.25 \pm 0.05$. The CSA in this range is found to be a function of AOD, where Eq. (11) is equal to zero.

Sensors are limited in sensitivity, which is defined by the noise equivalent reflectance difference NE$dR = R^{TOA} \cdot$ Noise/Signal (Schläpfer and Schaepman, 2002). Typical values of NEdR are found between 0.01 and roughly 0.002. $\pm$NEdR is an instrument specific envelope around the zero derivative of Eq. (11), where the aerosol induced signal is within the noise level and therefore impossible to be retrieved by the proposed method. See Seidel et al. (2008) for a further discussion on sensor performance requirements for AOD retrieval.

4.3.2. Influence of uncertainties in surface albedo

It follows from previous findings that the AOD retrieval is very sensitive to surface albedo, which is mostly not known *a priori* and has to be assumed by statistics, climatologies or retrieved by additional concurrent measurements. Airborne remote sensing campaigns (see *e.g.* Section 3.2) have the particular advantage that independent *in situ* measurements

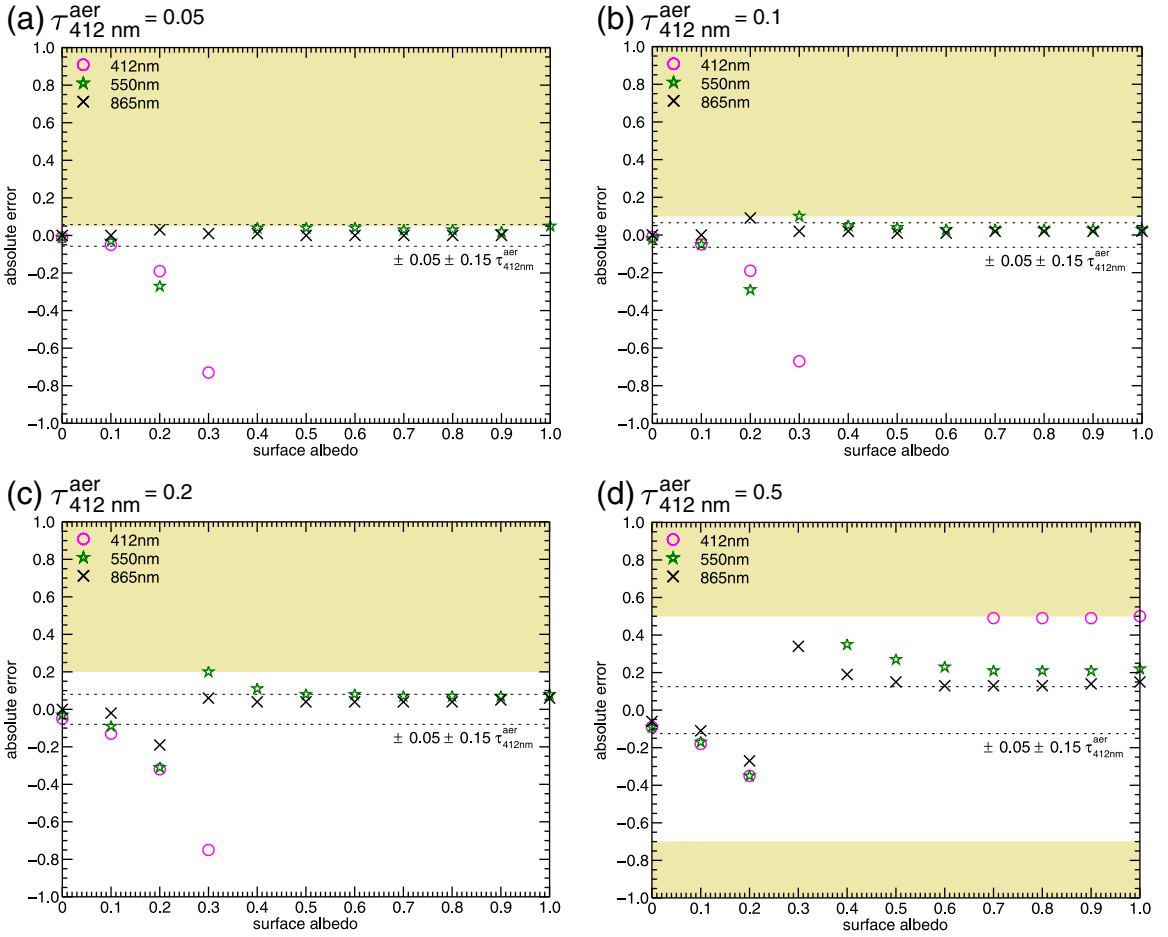

Fig. 7. Absolute error of AOD retrieval as a function of surface albedo. Calculations were performed using iSMART and compared to SCIATRAN. Retrievals in colored areas are not feasible because either $\tau^{aer}_{412nm} < 0$ or $\tau^{aer}_{412nm} > 1.2$. The dotted lines denote the expected uncertainty range of the MODIS dark-target ($0.01 \le a \le 0.25$) AOD retrieval.

from field spectrometers can be collected. Nevertheless, even these measurements have an individual uncertainty (Milton et al., 2009), which may bias the retrieval of AOD.

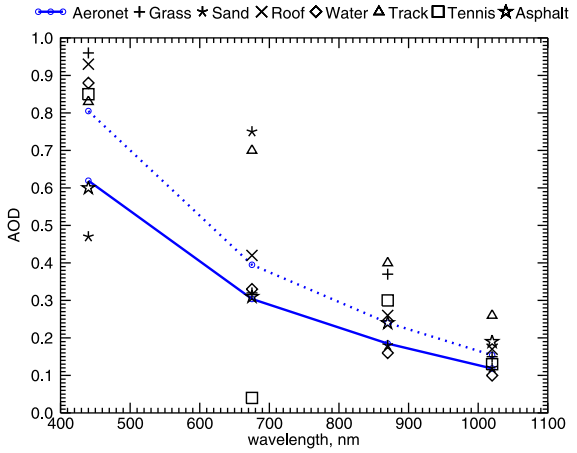

Fig. 8. Results of the AOD retrieval using APEX data on various in-situ reference targets. The solid line shows the AERONET reference AOD, which was measured on a nearby hill. The dotted line shows the extrapolated AOD, which corresponds to the elevation of the image data.

We analyze this effect using iSMART and show the results in Fig. 11. An uncertainty in a is simulated by a deviation d from the true surface albedo, such that $a_{error} = a_{true} \pm d$,

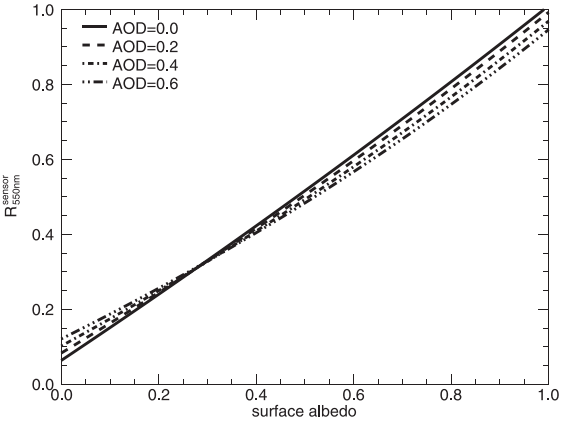

Fig. 9. Reflectance R^{TOA}_{550nm} using SMART (Eq. 2) with respect to surface albedo a at SZA = 60° for average continental aerosols and different AOD levels. Additional AOD increases R^{TOA}_{550nm} for $a < 0.3$ and *vice versa*. At $a \approx 0.3$ (critical surface albedo), R^{TOA}_{550nm} does not depend strongly on AOD.

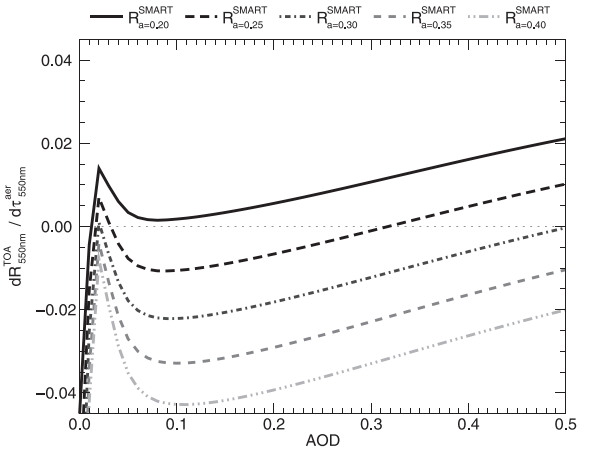

Fig. 10. Derivative of reflectance $R^{TOA}_{550\text{nm}}$ with respect to AOD according to Eq. (11). Positive values indicate an increase of R^{TOA}_{λ} for an increasing AOD, and *vice versa*. Values close to zero indicate a weak dependence of $R^{TOA}_{550\text{nm}}$ on AOD and therefore, a small uncertainty in $R^{TOA}_{550\text{nm}}$ translates into a large AOD uncertainty.

where $d \in [0.005, 0.01, 0.05]$. The results confirm that the AOD retrieval at dark surfaces ($a \leq 0.1$) is more robust to surface albedo uncertainties than at bright surfaces. An uncertainty of 1% ($d = 0.01$) leads to a difference in retrieved AOD of roughly 0.2 at a dark surface (see Fig. 11a). For $a \leq 0.3$, an overestimation of the surface albedo causes an overestimation of AOD. Retrievals at 400 nm and at SZA = 60° are more robust at dark targets than at 700 nm and at SZA = 30°. Some retrievals were even rejected at $a = 0.3$. It is obvious from Section 4.3.1 that even small uncertainties in surface albedo close to the CSA are leading to large variations in the retrieved AOD as shown in Fig. 11d. The errors at $d = 0$, $a = 0.4$ and SZA = 30° occurred because iSMART identified false local minima. In general, SZA = 30° was found to be more sensitive to surface albedo uncertainties than SZA = 60°.

5. Summary and conclusions

Fairly successful techniques and algorithms were developed for satellite aerosol remote sensing in the past three decades. Growing amounts of data are available for the study of aerosol distribution on the global scale. The corresponding advanced retrieval algorithms are often adapted for a specific satellite sensor and are mostly based on look-up-table approaches.

We therefore propose the fast, simple and flexible AOD retrieval algorithm iSMART. A short validation using synthetic data from SCIATRAN and airborne imaging spectrometer data from APEX have proven its feasibility. Retrieval errors using

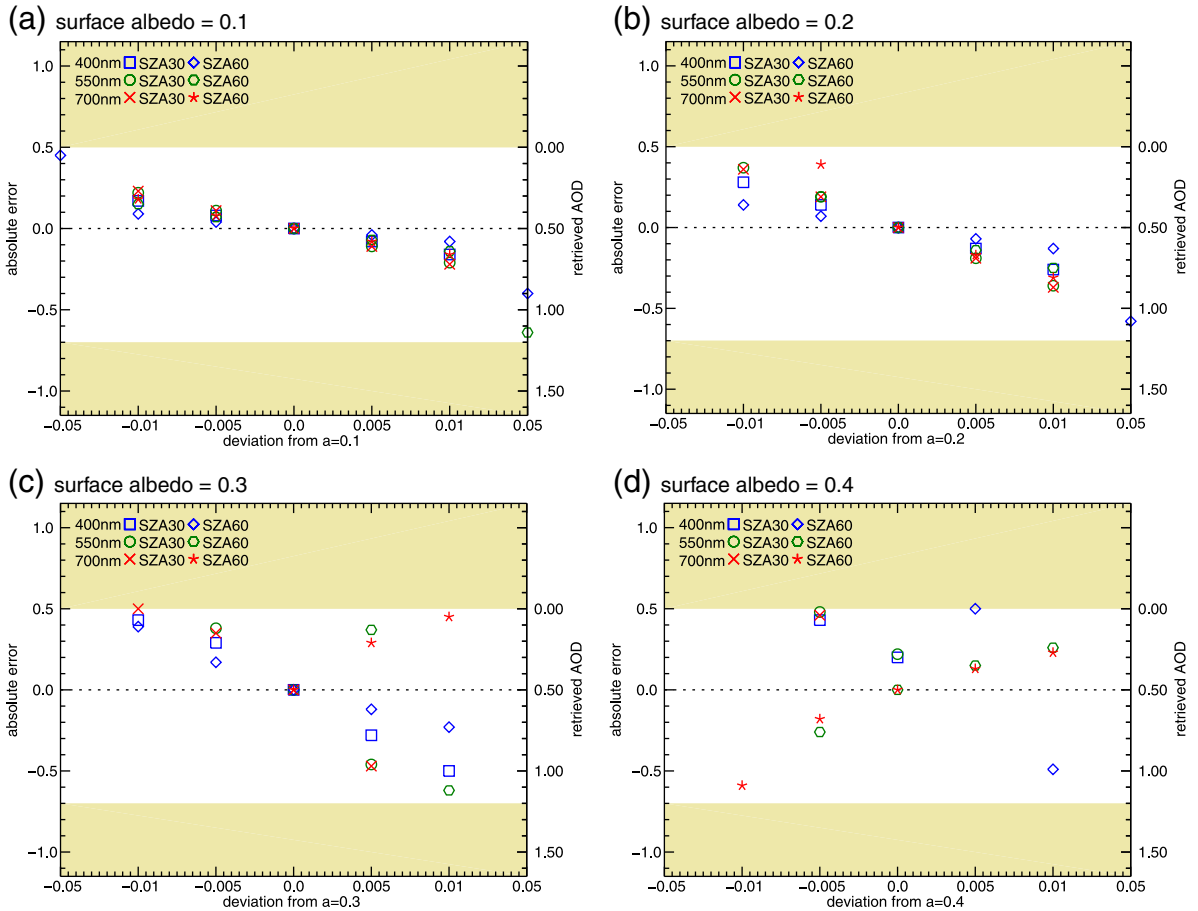

Fig. 11. Absolute error of AOD retrieval using iSMART as a function of surface albedo uncertainties at $\tau^{aer}_{412\text{nm}} = 0.5$. The uncertainties are simulated by a deviation from the true surface albedo. Retrievals in the colored areas are not feasible because either $\tau^{aer}_{412\text{nm}} < 0$ or $\tau^{aer}_{412\text{nm}} > 1.2$.

synthetic data were found to be in the same order of magnitude as the accuracy of the MODIS "dark target" AOD retrieval algorithm. The AOD retrieval using APEX data also generates promising results. The best retrieval accuracy is found in the near-infrared (*e.g.* 865 nm) for all surface albedo values using iSMART under the investigated conditions. The retrieval at 412 nm is less accurate due to neglected higher orders of aerosol scattering, as well as polarization and coupling of the aerosol–molecular scattering in the current version of SMART. Pronounced adjacency effects were observed by APEX due to haze in the lower atmosphere, which are not yet fully taken into account by SMART.

It was found that surface albedo and its associated uncertainty have a large influence on the AOD retrieval. A surface albedo between 0.25 and 0.4 can lead to large retrieval errors because the upwelling solar radiation does not depend strongly on AOD at the critical surface albedo (Fraser and Kaufman, 1985; Hsu et al., 2004; Popp et al., 2007; Seidel et al., 2008). It was found that an uncertainty in the surface albedo of 1% can translate in some cases to an AOD error of 0.2. The influence of uncertainties in the scattering phase function, size distribution and other parameters was not investigated.

Future versions of iSMART should account for three-dimensional radiative effects at the surface–atmosphere interface. Further extensions should comprise a statistically optimized inversion algorithm according to Dubovik et al. (2010), which would increase the retrieval accuracy and allow simultaneous retrievals of surface albedo and more complete aerosol properties. However, the latter requires multi-directional and polarized measurements to take advantage of the full information content of solar radiation.

We conclude that the proposed fast and simple algorithm is feasible for retrieving AOD with a promising accuracy from remote sensing data, given that the surface albedo is sufficiently known. iSMART is therefore particularly suited to applications requiring computational speed.

Acknowledgments

The work of A. A. Kokhanovsky was performed in the framework of DFG Project Terra. The Mie results were computed using a Mie code developed by the Sub-Department of Atmospheric, Oceanic and Planetary Physics, University of Oxford, UK. We thank C. Popp for the valuable discussions about the sensitivity of the surface albedo with regard to the aerosol retrieval. We also would like to thank the anonymous reviewers and A. Schubert for their valuable comments and suggestions, which helped to improve the manuscript.

References

Ångström, A., 1925. The albedo of various surfaces of ground. Geogr. Ann. 7, 323–342.
Ångström, A., 1930. On the atmospheric transmission of sun radiation. II. Geogr. Ann. 12, 130–159.
Bassani, C., Cavalli, R.M., Pignatti, S., 2010. Aerosol optical retrieval and surface reflectance from airborne remote sensing data over land. Sensors 10 (7), 6421–6438.
Berk, A., Bernstein, L., Robertson, D., 1989. MODTRAN: a moderate resolution model for LOWTRAN7. Tech. Rep. GL-TR-89-0122. Air Force Geophysics Lab, Hanscom AFB, Massachusetts, USA.
Chandrasekhar, S., 1960. Radiative Transfer. Dover, New York, USA.
Charlson, R., Schwartz, S., Hales, J., Cess, R., Coakley, J., Hansen, J., Hofmann, D., 1992. Climate forcing by anthropogenic aerosols. Science 255, 423–430.
Diner, D.J., Martonchik, J.V., Kahn, R.A., Pinty, B., Gobron, N., Nelson, D.L., Holben, B.N., 2005. Using angular and spectral shape similarity constraints to improve MISR aerosol and surface retrievals over land. Remote Sens. Environ. 94 (2), 155–171.
Dubovik, O., King, M.D., 2000. A flexible inversion algorithm for retrieval of aerosol optical properties from sun and sky radiance measurements. J. Geophys. Res. D105 (16), 20673–20696.
Dubovik, O., Herman, M., Holdak, A., Lapyonok, T., Tanré, D., Deuzé, J.L., Ducos, F., Sinyuk, A., Lopatin, A., 2010. Statistically optimized inversion algorithm for enhanced retrieval of aerosol properties from spectral multi-angle polarimetric satellite observations. Atmos. Meas. Tech. Discuss. 3 (6), 4967–5077.
Fraser, R., Kaufman, Y., 1985. The relative importance of aerosol scattering and absorption in remote sensing. IEEE Trans. Geosci. Remote Sens. GE-23 (5), 625–633 (sep.).
Gao, B.-C., Montes, M.J., Davis, C.O., Goetz, A.F.H., 2009. Atmospheric correction algorithms for hyperspectral remote sensing data of land and ocean. Remote Sens. Environ. 113 (Supplement 1), S17–S24 (9).
Guanter, L., Alonso, L., Moreno, J., 2005. A method for the surface reflectance retrieval from proba/chris data over land: application to ESA SPARC campaigns. IEEE Trans. Geosci. Remote Sens. 43 (12), 2908–2917.
Hansen, J.E., Travis, L.D., 1974. Light scattering in planetary atmospheres. Space Sci. Rev. 16, 527–610.
Holben, B., Eck, T., Slutsker, I., Tanré, D., Buis, J., Setzer, A., Vermote, E., Reagan, J., Kaufman, Y., Nakajima, T., Lavenu, F., Jankowiak, I., Smirnov, A., 1998. AERONET — a federated instrument network and data archive for aerosol characterization. Remote Sens. Environ. 66 (1), 1–16.
Hsu, N.C., Tsay, S.-C., King, M.D., Herman, J.R., 2004. Aerosol properties over bright-reflecting source regions. IEEE Trans. Geosci. Remote Sens. 42 (3), 557–569.
Itten, K.I., Schaepman, M.E., Vos, L.D., Hermans, L., Schlaepfer, H., Droz, F., 1997. APEX — airborne prism experiment a new concept for an airborne imaging spectrometer. Third International Airborne Remote Sensing Conference and Exhibition. Vol. 1. Copenhagen, Denmark, pp. 181–188.
Itten, K.I., Dell'Endice, F., Hueni, A., Kneubühler, M., Schläpfer, D., Odermatt, D., Seidel, F., Huber, S., Schopfer, J., Kellenberger, T., Bühler, Y., D'Odorico, P., Nieke, J., Alberti, E., Meuleman, K., 2008. APEX — the hyperspectral ESA airborne prism experiment. Sensors 8 (10), 6235–6259.
Katsev, I.L., Prikhach, A.S., Zege, E.P., Grudo, J.O., Kokhanovsky, A.A., 2010. Speeding up the aerosol optical thickness retrieval using analytical solutions of radiative transfer theory. Atmos. Meas. Tech. 3 (5), 1403–1422.
Kokhanovsky, A.A., 2006. Cloud optics. Atmospheric and Oceanographic Sciences Library, Vol. 34. Springer.
Kokhanovsky, A.A., 2008. Aerosol Optics — Light Absorption and Scattering by Particles in the Atmosphere. Springer Praxis Books, Springer Berlin Heidelberg.
Kokhanovsky, A.A., de Leeuw, G.D., 2009. Satellite aerosol remote sensing over land. Environmental Sciences. Springer Praxis Books.
Kokhanovsky, A.A., Mayer, B., Rozanov, V.V., 2005. A parameterization of the diffuse transmittance and reflectance for aerosol remote sensing problems. Atmos. Res. 73 (1–2), 37–43.
Kokhanovsky, A.A., Budak, V.P., Cornet, C., Duan, M., Emde, C., Katsev, I.L., Klyukov, D.A., Korkin, S.V., C-Labonnote, L., Mayer, B., Min, Q., Nakajima, T., Ota, Y., Prikhach, A.S., Rozanov, V.V., Yokota, T., Zege, E.P., 2010a. Benchmark results in vector atmospheric radiative transfer. J. Quant. Spectrosc. Radiat. Transf. 111 (12–13), 1931–1946.
Kokhanovsky, A.A., Deuzé, J.L., Diner, D.J., Dubovik, O., Ducos, F., Emde, C., Garay, M.J., Grainger, R.G., Heckel, A., Herman, M., Katsev, I.L., Keller, J., Levy, R., North, P.R.J., Prikhach, A.S., Rozanov, V.V., Sayer, A.M., Ota, Y., Tanré, D., Thomas, G.E., Zege, E.P., 2010b. The inter-comparison of major satellite aerosol retrieval algorithms using simulated intensity and polarization characteristics of reflected light. Atmos. Meas. Tech. 3 (4), 909–932.
Levy, R.C., Remer, L.A., Mattoo, S., Vermote, E.F., Kaufman, Y.J., 2007. Second-generation operational algorithm: retrieval of aerosol properties over land from inversion of moderate resolution imaging spectroradiometer spectral reflectance. J. Geophys. Res. 112 (D13211).
Levy, R.C., Remer, L.A., Tanré, D., Mattoo, S., Kaufman, Y.J., 2009. Algorithm for remote sensing of tropospheric aerosol over dark targets from MODIS: collections 005 and 051: revision 2. Tech. rep., NASA/GSFC.
Levy, R.C., Remer, L.A., Kleidman, R.G., Mattoo, S., Ichoku, C., Kahn, R., Eck, T.F., 2010. Global evaluation of the collection 5 MODIS dark-target aerosol products over land. Atmos. Chem. Phys. 10 (21), 10399–10420.
Lyapustin, A., 2001. Three-dimensional effects in the remote sensing of surface albedo. IEEE Trans. Geosci. Remote Sens. 39 (2), 254–263.
Martonchik, J.V., Kahn, R.A., Diner, D.J., 2009. Retrieval of aerosol properties over land using MISR observations. In: Kokhanovsky, A.A., de Leeuw, G. (Eds.), Satellite Aerosol Remote Sensing over Land. Springer Berlin Heidelberg.

Milton, E.J., Schaepman, M.E., Anderson, K., Kneubühler, M., Fox, N., 2009. Progress in field spectroscopy. Remote Sens. Environ. 113 (Supplement 1), S92–S109.

Popp, C., Riffler, R., Hauser, A., Wunderle, S., 2007. Approximation of aerosol type over land surfaces from msg-seviri data. Joint 2007 EUMETSAT Meteorological Satellite Conference and the 15th Satellite Meteorology and Oceanography Conference of the American Meteorological Society, Amsterdam, the Netherlands.

Remer, L., Kaufman, Y., Tanré, D., Mattoo, S., Chu, D., Martins, J., Li, R., Ichoku, C., Levy, R., Kleidman, R., Eck, T., Vermote, E., Holben, B., 2005. The MODIS aerosol algorithm, products, and validation. J. Atmos. Sci. 62 (4), 947–973.

Rind, D., Chin, M., Feingold, G., Streets, D., Kahn, R.A., Schwartz, S.E., Yu, H., 2009. Modeling the effects of aerosols on climate. Atmospheric Aerosol Properties and Impacts on Climate. A Report by the U.S. Climate Change Science Program and the Subcommittee on Global Change Research. National Aeronautics and Space Administration, Washington, D.C., USA.

Rozanov, V.V., Kokhanovsky, A.A., 2006. The solution of the vector radiative transfer equation using the discrete ordinates technique: Selected applications. Atmos. Res. 79 (3–4), 241–265.

Rozanov, A., Rozanov, V., Buchwitz, M., Kokhanovsky, A., Burrows, J., 2005. SCIATRAN 2.0 — a new radiative transfer model for geophysical applications in the 175–2400 nm spectral region. Adv. Space Res. 36 (5), 1015–1019.

Ruckstuhl, C., Philipona, R., Behrens, K., Collaud Coen, M., Dürr, B., Heimo, A., Mätzler, C., Nyeki, S., Ohmura, A., Vuilleumier, L., Weller, M., Wehrli, C., Zelenka, A., 2008. Aerosol and cloud effects on solar brightening and the recent rapid warming. Geophys. Res. Lett. 35 (12).

Schaepman, M.E., Schläpfer, D., Itten, K.I., 1998. APEX — airborne prism experiment: an airborne imaging spectrometer serving as a precursor instrument of the future ESA land surface processes interactions mission. 1st Intl. EARSeL Workshop on Imaging Spectroscopy. EARSeL, Paris, pp. 45–52.

Schläpfer, D., Schaepman, M., 2002. Modeling the noise equivalent radiance requirements of imaging spectrometers based on scientific applications. Appl. Opt. 41 (27), 5691–5701.

Seidel, F., Schläpfer, D., Nieke, J., Itten, K., 2008. Sensor performance requirements for the retrieval of atmospheric aerosols by airborne optical remote sensing. Sensors 8 (3), 1901–1914.

Seidel, F.C., Kokhanovsky, A.A., Schaepman, M.E., 2010. Fast and simple model for atmospheric radiative transfer. Atmos. Meas. Tech. 3 (4), 1129–1141.

Sobolev, V.V., 1972. Light Scattering in Planetary Atmospheres. Nauka, Moscow.

Solomon, S., Qin, D., Manning, M., Chen, Z., Marquis, M., Averyt, K., Tignor, M., Miller, H. (Eds.), 2007. Climate Change 2007: The Physical Science Basis. Contribution of Working Group I to the Fourth Assessment Report of the Intergovernmental Panel on Climate Change. Cambridge University Press, Cambridge, United Kingdom and New York, NY, USA.

Stamnes, K., Tsay, S.-C., Wiscombe, W., Jayaweera, K., 1988. Numerically stable algorithm for discrete-ordinate-method radiative transfer in multiple scattering and emitting layered media. Appl. Opt. 27 (12), 2502.

Tanré, D., 2010. Derivation of tropospheric aerosol properties from satellite observations. C. R. Geoscience 342 (4–5), 403–411.

Torres, O., Tanskanen, A., Veihelmann, B., Ahn, C., Braak, R., Bhartia, P.K., Veefkind, P., Levelt, P., 2007. Aerosols and surface UV products from ozone monitoring instrument observations: an overview. J. Geophys. Res. 112 (D24).

van de Hulst, H.C., 1948. Scattering in a planetary atmosphere. Astrophys. J. 107, 220–246.

Vermote, E.F., Tanré, D., Deuzé, J.L., Herman, M., Morcrette, J.-J., 1997. Second simulation of the satellite signal in the solar spectrum, 6S: an overview. IEEE Trans. Geosci. Remote Sens. 35 (3), 675–686.

Wilson, R., Spengler, J.D., 1996. Particles in Our Air: Concentrations and Health Effects. Harvard University Press, Cambridge, Massachusetts, USA.

Zhu, L., Martins, J.V., Remer, L.A., 2011. Biomass burning aerosol absorption measurements with MODIS using the critical reflectance method. J. Geophys. Res. 116. (D7).